Fuel 276 (2020) 118143

Contents lists available at ScienceDirect

Fuel

journal homepage: www.elsevier.com/locate/fuel

Full Length Article

# $CO_2$ adsorption capacity of zeolites synthesized from coal fly ashes

Thiago F. de Aquino[a,*], Sabrina T. Estevam[a], Vanessa O. Viola[a], Carolina R.M. Marques[a], Fernando L. Zancan[a], Lídia B. Vasconcelos[b], Humberto G. Riella[c], Marçal J.R. Pires[d], Rafael Morales-Ospino[e], A. Eurico B. Torres[e], Moises Bastos-Neto[e], Célio L. Cavalcante Jr.[e]

[a] Beneficent Association of the Santa Catarina Coal Industry (SATC), Pascoal Meller St. 73, 88805-380 Criciúma, Brazil
[b] Eneva S.A., Praia de Botafogo 501, 22250-040 Rio de Janeiro, Brazil
[c] Materials and Corrosion Laboratory, Department of Chemical Engineering and Food Engineering, Federal University of Santa Catarina (UFSC), University Campus, 88040-900 Florianópolis, Brazil
[d] Post-Graduation Program in Engineering and Technology Materials, Pontifical Catholic University of Rio Grande do Sul (PUCRS), Av. Ipiranga 6681, 90619-900 Porto Alegre, Brazil
[e] Adsorption Separation Research Group, Department of Chemical Engineering, Federal University of Ceará (UFC), Pici Campus, 60455-760 Fortaleza, Brazil

ARTICLE INFO

*Keywords:*
Fly ash conversion
Zeolite synthesis
$CO_2$ capture
Adsorption cycles

ABSTRACT

Given the increase in $CO_2$ emissions, the adsorption process using zeolites are proposed to remove this compound from combustion gases in pulverized coal power plants. Besides it, these materials can also be synthesized using coal fly ash to reconcile environmental and economic concerns. The aim of this study was to measure the adsorption capacity of zeolites synthesized from coal fly ash compared with commercial zeolites and assess their performance in temperature swing adsorption processes. Two pelletized synthetic zeolites were selected, one NaX type (SZX) and one NaA type (SZA), and two commercial zeolites, one NaX (CZX) and one NaA (CZA). Zeolites were characterized by XRF, XRD and textural analysis (BET). Adsorption capacity tests were performed by thermogravimetric analysis using similar $CO_2$ concentrations to those found in pulverized carbon combustion gases, without moisture. Isotherms were also obtained for synthetic and commercial zeolites type X. The XRD results showed substantial similarity between the commercial and synthesized zeolites, indicating a good degree of crystallinity. The $CO_2$ adsorption capacity at 303 K for both samples showed values similar to those reported in the literature (1.97 mmol/g for SZX and 1.37 mmol/g for SZA), demonstrating their potential in commercial applications. After five cycles, the adsorption capacity of all samples remained practically unchanged, indicating the possibility of application in TSA processes. In the adsorption tests at different temperatures and in the isotherms, adsorption capacity declined as temperature increased for both samples, being similar to benchmark commercial 13X and 4A zeolite adsorbents.

## 1. Introduction

The environmental pollution caused by high greenhouse gas (GHG) emissions has gained greater visibility in recent years [1,2]. Carbon dioxide stands out as the greatest source of anthropogenic emissions, associated primarily with the burning of fossil fuels [3,4]. As such, post-combustion $CO_2$ capture in power plants is an emerging demand and challenging in terms of developing technically and economically viable technologies [2].

The most well-developed industrial $CO_2$ capture processes occur via absorption, with ammonia standing out among the solvents used due to its easy reaction with $CO_2$ via rapid bonding, even at low partial pressures. However, despite its efficient $CO_2$ removal, this technique can be improved, particularly in relation to the regeneration costs of the absorbent material [1–3]. Additional problems that raise capital and operating costs include thermal and oxidative degradation of solvents, solvent losses via volatilization and corrosion [4].

As a result, alternative capture processes have been increasingly studied, including pressure (PSA) and temperature swing adsorption (TSA) [5]. Processes involving adsorption are recommended as functional techniques with significant economic advantages, largely due to their low energy demand per metric ton of $CO_2$ captured [3]. Adsorption processes are also beneficial because of their high $CO_2$ capacity and selectivity in gaseous mixtures containing nitrogen, oxygen, methane and hydrogen; good mechanical properties of the adsorbents; easy regeneration and the ability to act in adsorption/desorption cycles [6,7].

* Corresponding author.
*E-mail address:* thiago.aquino@satc.edu.br (T.F.d. Aquino).

https://doi.org/10.1016/j.fuel.2020.118143
Received 31 May 2019; Received in revised form 24 January 2020; Accepted 16 May 2020
Available online 22 May 2020

Microporous materials, such as zeolites, can be applied in various industrial processes as in advanced ceramic coatings [8], removal of contaminants from liquid effluents [2,9–11], catalysis [12,13], detergent additives [14,15] and fertilizers [16,17]. And in the context of gas adsorption, particularly $CO_2$ capture, these materials stand out for their use as adsorbents [1,6,18,19]. Their high adsorption capacity is the result of low density, large volume of empty spaces (when dehydrated), high crystalline structure stability and uniformly sized channels [3,19].

Among the different classes of zeolites, types NaX and NaA are the most well-known in the field of $CO_2$ capture, exhibiting high selectivity in relation to other gases [1,7,18,20,21]. These zeolites are differentiated according to their structure and Si/Al molar ratio, with zeolite X exhibiting a ratio between 1.0 and 1.5 and zeolite A 1.0 [22].

Nevertheless, the progression of adsorption processes is dependent on the availability of low-cost adsorbents, high adsorption capacity and dynamics, and the substantial selective power of these materials [5]. To achieve this viability, studies about synthetic zeolites have been made using different industrial wastes [2,21,23–25]. Among these wastes, coal fly ash is one of the most used materials to synthesize zeolites, and already shows promising results, in some cases can reduce the costs around 40% [5,7,19,26–32]. Its good application is the result of high concentration of silicon and aluminium in the fly ash and the low presence of organic materials [7,19,28,29].

In addition to this, Brazilian coals have around 20–50% of ashes [33], therefore, its consumption generates significant amounts of ashes [27,18]. Furthermore, coal is the primary source of electrical energy production worldwide and its use has grown sharply since 2003 [26]. The industry cannot consume the entire volume of ashes generated, since less than 45% of the total amount of ashes produced in Brazil are reused, particularly in the cement industry [18,21,34]. It creates a demand for more economically and environmentally adequate solutions for these wastes [26,29,30,33].

In order to be applied in industrial adsorption processes, zeolites may not be in powder form, as synthesized, but in pellet form or appropriately sized spheres [35,36]. The conformation of these adsorbent materials is crucial to industrial applications and the products of this process must exhibit high porosity to maintain the properties of the adsorbent [3]. The material used in conformation can significantly influences its intracrystalline features and affects the adsorption properties of the final material [36].

In light of the above, the primary objective of this study was to assess the $CO_2$ adsorption capacity of zeolites synthesized from coal fly ash and compare it to commercial zeolites applied under the same conditions. The possibility of regenerating these materials by applying several adsorption/desorption cycles was also assessed to verify their possible applications in a TSA process. In addition the influence of temperature on adsorption capacity was also evaluated.

## 2. Materials and methods

Two fly ash samples were used in this study, one collected at the outlet of the electrostatic precipitator of unit C at the Jorge Lacerda power plant in the city of Capivari de Baixo (Santa Catarina state, Brazil), and the other from the silos at the Pecém II power plant in Fortaleza (Ceará state, Brazil) under flue-gas desulfurization (FGD). Distilled water was used in all stages of the synthesis process and the other reactants were all analytical grade.

### 2.1. Zeolite synthesis from coal fly ash

In the present study, zeolites types NaX and NaA were synthesized from coal fly ash, based on previous studies, where the parameters of the processes have been already optimized [7,28]. The syntheses were carried out by a two-step process consisting of prior fusion of the ash with sodium hydroxide (NaOH) and subsequent hydrothermal reaction.

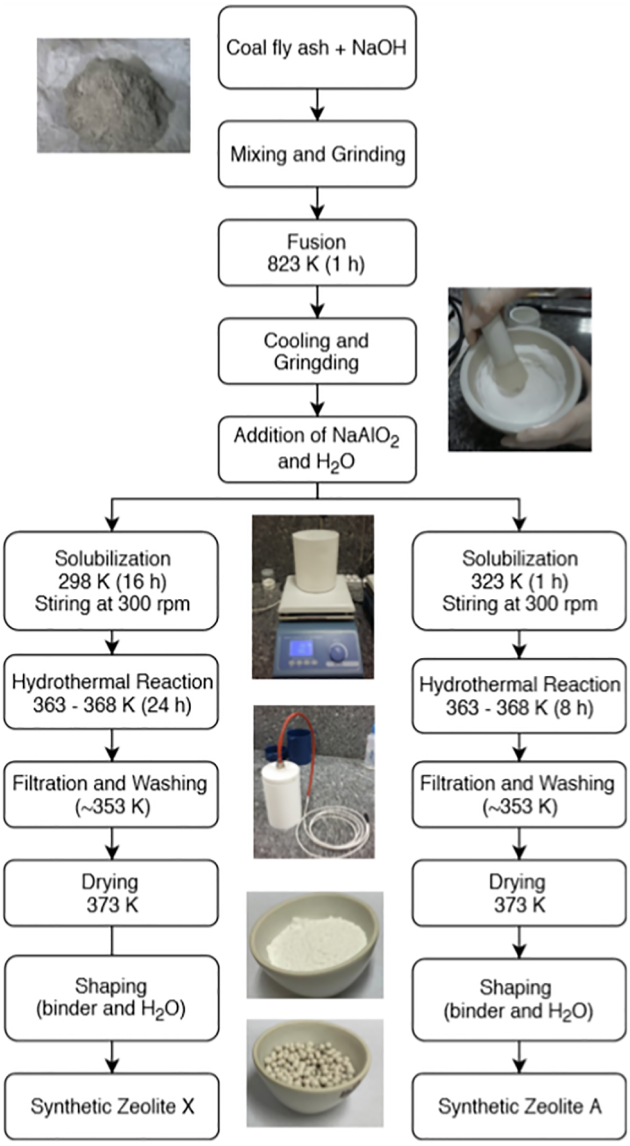


**Fig. 1.** Basic zeolite synthesis procedure.

The flowchart in Fig. 1 shows the synthesis steps to obtain zeolites types NaA and NaX. To determine the molar ratio of the synthetic zeolites was necessary to characterize the coal fly ashes using XRF and XRD technics. Then, considering the chemical reactants ($H_2O$, NaOH e $NaAlO_2$) and the amorphous content of silicium and aluminium in the fly ashes, it was possible to determine the main molar ratio of the oxides utilized in the zeolites syntheses processes. The ratios used for zeolite SZX were $SiO_2/Al_2O_3$ = 3.5; $Na_2O/SiO_2$ = 2.05; and $H_2O/Na_2O$ = 51.4, and for synthetic zeolite SZA $SiO_2/Al_2O_3$ = 1.0; $Na_2O/SiO_2$ = 3.25; and $H_2O/Na_2O$ = 80.4.

To synthesize both samples, the fusions of the fly ashes with NaOH were carried out at 823 K for 1 h. After cooling, the samples were grinded and $NaAlO_2$ and $H_2O$ were added. Both samples were homogenized by agitation at 300 rpm. For zeolite type NaX, the solubilization was carried out at room temperature for 16 h, and for type NaA this step was proceeded at 323 K for 1 h.

After the solubilization step, the hydrothermal reactions were performed in a static PTFE reactor with controlled temperature between 363 and 368 K during 24 h to zeolite type NaX and 8 h to zeolite type NaA. The temperature was controlled by a thermocouple PT100 type inserted into the reactor. This temperature control is really important to avoid the formation of other types of zeolites [23,37].

**Table 1**
Chemical composition of the major elements in the ash used for synthesis on a per mass basis and in the form of oxides.

| Composition (wt %) | $SiO_2$ | $Al_2O_3$ | $Na_2O$ | $Fe_2O_3$ | MgO | CaO | $TiO_2$ | $K_2O$ | $SO_3$ | $P_2O_5$ | LOI |
|---|---|---|---|---|---|---|---|---|---|---|---|
| Jorge Lacerda Ash | 60.76 | 25.48 | 0.56 | 5.00 | 0.79 | 1.54 | 1.11 | 2.91 | 0.47 | 0.07 | 1.33 |
| Pecém Ash | 49.96 | 21.14 | 1.85 | 8.66 | 3.33 | 6.73 | 0.86 | 1.80 | 1.61 | 0.14 | 3.95 |

* LOI – Loss on ignition.

After the process, the synthetic zeolites were shaped in spherical form with 8% of bentonite e 35% of $H_2O$, using a Caleva struder/spheronizer, Multilab model. The samples were characterized according to their main properties, including chemical, mineralogical and morphological analyses as described below.

### 2.2. Characterization of the ashes and zeolites

#### 2.2.1. Chemical, mineralogical and morphological composition

Chemical composition was determined by X-ray fluorescence (XRF) in all the samples (pressed tablets), using an energy-dispersive X-ray fluorescence spectrometer (Shimadzu EDX 7000). Prior to these analyses, loss on ignition (LOI) testing was conducted based on the procedure described in ASTM D7348-07.

The mineral composition of the fly ash samples was quantitatively analyzed by powder diffraction, in a Philips X-ray diffractometer (MPD 1880). Phases were identified using the ICDD (International Center for Diffraction Data, 2003) PDF2 database and PAN-ICSD (PANanalytical Inorganic Crystal Structure Database, 2007), and quantified via the Rietveld method using crystalline structures from the ICSD database (2007) and 10% fluorite ($CaF_2$) as internal standard to help calculate the amorphous phase.

Qualitative mineralogical analyses of fused samples and synthesized zeolites were also performed using the powder method, in an X-ray diffractometer (Shimadzu, LabX XRD 6100), and phase identification with the aid of the COD (Crystallography Open Database, 2016) and Match!3 software.

In order to assess morphology, the samples were previously coated with gold-palladium (Au/Pd) and analyzed by scanning electron microscopy (SEM) (Zeiss EVO 10).

#### 2.2.2. Textural properties and thermogravimetric analysis

Textural analyses were carried out using the nitrogen ($N_2$) adsorption technique, in a surface area and pore size analyzer (Quantachrome Instruments, Quadrasorb EVO). Information on the surface area (calculated via the BET method), pore volume and diameter were obtained with Quantachrome QuadraWin software.

The adsorption capacity of the samples was determined by thermogravimetric analysis (TGA), using a Discovery SDT 650 simultaneous TGA-DSC instrument (TA Instruments).

Considering the application of the zeolites in TSA process operating in atmospheric pressure, the adsorption capacity of the samples was assessed in five adsorption/desorption cycle using a 7% $CO_2/N_2$ v/v gas mixture without the presence of water, at an adsorption temperature of 303 K and ambient pressure (1.01 bar). Analysis was conducted in stages, as follows:

a) Pretreatment at 723 K for 30 min and a flow rate of 100 mL/min of $N_2$ for sample activation;
b) Gas exchange of $N_2$ for a 14% $CO_2/N_2$ mixture at 100 mL/min, producing a 7% $CO_2$ chain, for 20 min (after equilibrium) at 303 K for the adsorption stage;
c) Further exchange to a $N_2$ atmosphere at 100 mL/min for 10 min and heating up to 573 K with a 30 min plateau for $CO_2$ desorption;
d) Repetition of steps b and c four more times.

Adsorption capacity at different temperatures was assessed in three adsorption cycles, following the same steps described above except the adsorption temperature (step b) was changed to 323 K, 348 K and 373 K. The average value of three readings was used.

#### 2.2.3. Pure $CO_2$ adsorption isotherms

The experimental adsorption isotherms were obtained using a magnetic suspension balance Rubotherm (Bochum, Germany). The pure $CO_2$ equilibrium measurements were performed at three temperature values (323, 343 and 363 K) for both the commercial and synthesized adsorbent samples. Between 0.5 and 1 g of each sample was placed inside the balance and outgassed prior the experiment at 573 K under vacuum during 10 h. Afterwards the adsorbent sample was cooled down to the experiment temperature while the gas pressure was increased stepwise until 1 bar. The mass variation was recorded constantly for each pressure level until achieving the equilibrium condition (mass variation $< 10^{-4}$ g for at least 30 min).

## 3. Results and discussion

### 3.1. Chemical and mineralogical characterization of ashes

The chemical compositions of the major elements in the two fly ash samples studied are shown in Table 1. The main differences between the two materials are the higher silicon and aluminum concentrations in the Jorge Lacerda sample (> 85%) and its lower unburned carbon and iron content, which is a good sign since these factors compromise high-quality zeolite formation from coal fly ash, particularly for type X zeolites [7]. The high calcium and magnesium oxide concentration in the fly ash from Pecém can be explained by its exposure to flue-gas desulfurization (FGD), whereby flue gases are absorbed using a lime solution to remove sulfur dioxide. Additionally, hydrothermal synthesis with prior fusion produced a good quality type X zeolite (SZX) from ashes collected at the Jorge Lacerda power plant, but not that obtained at the Pecém plant, although the latter did produce a synthetic type A zeolite (SZA).

X-ray diffraction (XRD) is one of the best techniques to characterize ash used in synthesis processes. The mineralogy results of both ash samples are displayed in Fig. 2, indicating the presence of halos typical of materials with a high amorphous content, such as coal fly ash. Although both samples contain the same mineralogical phases, quartz, mullite and hematite, the Jorge Lacerda fly ash exhibits more intense phase peaks, indicating a high crystalline content (26%). The results of quantitative analysis of the phases using the Rietveld method are shown in Table 2, demonstrating a higher amorphous content in the Pecém fly ash (85%). In order to select the best zeolite synthesis method, it is important to know the crystalline phases present in the initial material.

The fusion method is generally applied to facilitate decomposition of Si and Al-rich crystalline phases and form soluble aluminates and silicates, which are highly reactive and favor zeolite formation [28]. The XRD patterns of the mixtures (ash and NaOH) after the fusion step are presented in Fig. 3.

Before fusion, both ashes had the same phases (quartz, mullite and hematite) that are stable phases of silicon, aluminum and iron. After fusion it can be seen that these phases were transformed into more reactive silicates and aluminates that can be more easily rearranged during zeolite synthesis [28,38].

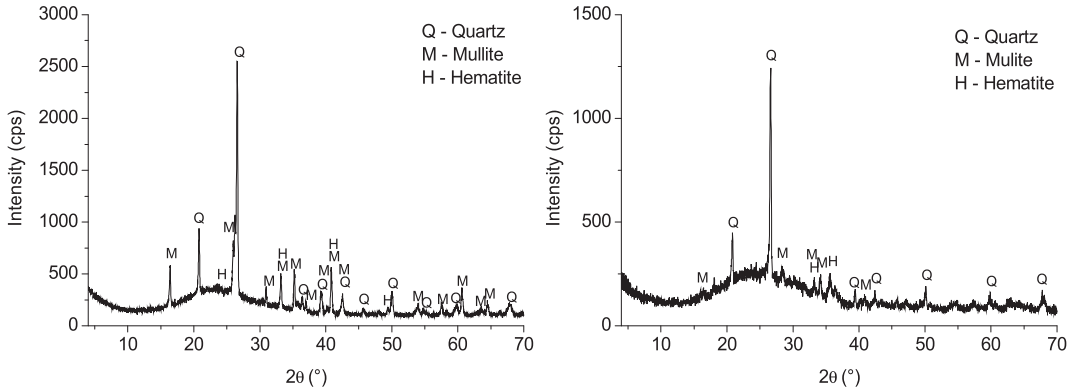


**Fig. 2.** Diffractogram of the (a) Jorge Lacerda and (b) Pecém fly ash samples.

**Table 2**
Quantification of the phases present in the Jorge Lacerda and Pecém fly ash with lime.

| State | Phases | %wt, Jorge Lacerda ash | %wt, Pecém ash |
|---|---|---|---|
| Amorphous | – | 74 | 85 |
| Crystalline | Quartz | 9 | 8 |
| | Mullite | 16 | 2 |
| | Magnesioferrite | – | 2 |
| | Hematite | – | 3 |
| | Magnetite | 1 | – |

### 3.2. Chemical and mineralogical composition of the zeolites

The chemical composition of commercial type X (CZX) and A zeolites (CZA) and those synthesized from coal fly ash obtained at the Jorge Lacerda (type X – SZX) and Pecém (type A – SZA) power plants are shown in Table 3. The $SiO_2/Al_2O_3$ molar ratios for the synthesized zeolites (3.01–3.44) are close to the ranges indicated for the respective zeolite types [22]. Based on the diffractograms of the commercial and synthetic type X zeolites, shown in Fig. 4 (a) and (b), respectively, the formation of type X zeolites was good in the sample synthesized from coal fly ash when compared to the commercial material. The low background and high intensity of the peaks demonstrates good crystallinity in phase formation, especially for zeolite X. The presence of zeolite A impurities is evident in both samples, as well as minor zeolite sodalite contamination in the synthetic zeolite, making it possible to infer equal quality for both the commercial and synthetic zeolite.

The diffractograms for the type A zeolites (Fig. 5 (a) and (b)) indicate similar behavior, with quartz impurities in both samples and sodalite in the synthetic sample. The presence of quartz in the synthetic zeolite can be attributed to the remaining content of this phase in the fly ash even after fusion. The more intense zeolite A peaks in the commercial sample demonstrate better formation in relation to the synthetic material; however, the sample obtained from fly ash collected at the Pecém power plant exhibits good quality, confirmed by the low background and high intensity peaks.

**Table 3**
Chemical composition of the major elements in the commercial and synthetic zeolites.

| Composition (wt%) | CZX | SZX | CZA | SZA |
|---|---|---|---|---|
| $SiO_2$ | 43.35 | 39.90 | 48.95 | 37.79 |
| $Al_2O_3$ | 21.45 | 22.57 | 27.39 | 23.60 |
| $Na_2O$ | 7.39 | 11.29 | 9.19 | 6.83 |
| $Fe_2O_3$ | 1.71 | 6.68 | 1.67 | 9.05 |
| MgO | 1.16 | < 0.01 | 1.91 | 0.75 |
| CaO | 0.70 | 2.14 | 2.26 | 5.59 |
| $TiO_2$ | 0.23 | 1.52 | 0.20 | 1.04 |
| $K_2O$ | 0.81 | 1.44 | 1.04 | 0.69 |
| $SO_3$ | 0.21 | 0.15 | 0.14 | 0.38 |
| Minor elements | 0.05 | 0.21 | 0.04 | 0.17 |
| LOI | 22.94 | 14.10 | 7.20 | 14.10 |
| $SiO_2/Al_2O_3$ (molar) | 3.44 | 3.01 | 3.04 | 2.72 |

* LOI – Loss on ignition.

### 3.3. Morphological analysis of the ash and synthesized zeolites

The morphology of coal fly ash from the Jorge Lacerda and Pecém power plants is shown in Fig. 6 (a) and (b), respectively. The well-

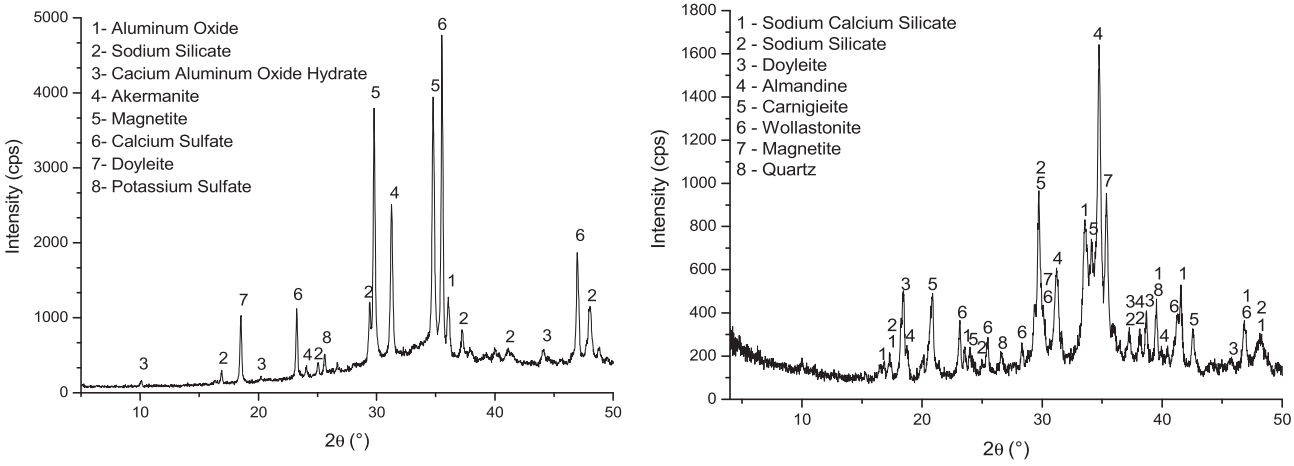


**Fig. 3.** Diffractogram of the (a) Jorge Lacerda and (b) Pecém fly ash samples after fusion.

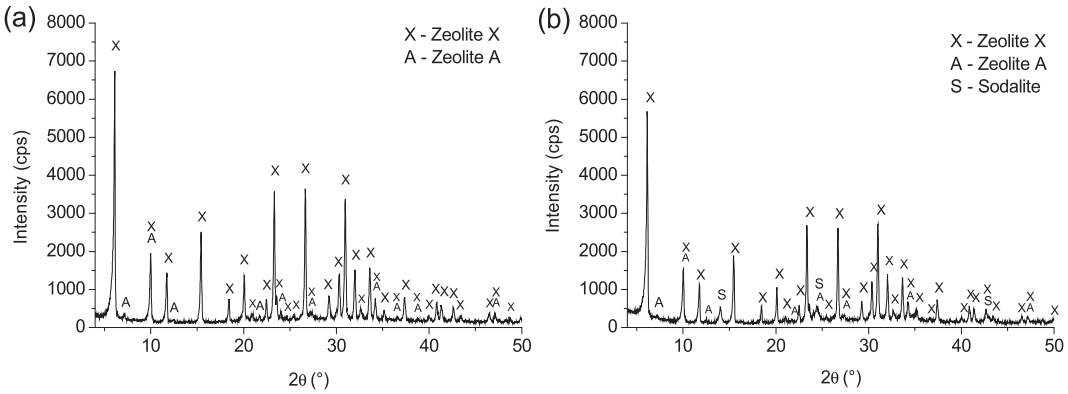


**Fig. 4.** X-ray diffractograms of the 13X (a) CZX and (b) SZX zeolites.

defined spherical shape of both samples is typical of fly ash particles [7,28] and their greater sphericity can be attributed to their amorphous coating formed as a result of relatively abrupt cooling after combustion [39].

The morphology of the synthetic X and A zeolites are presented in Fig. 7. The typical octahedral prism shape observed in sample SZX (Fig. 7 (a)) confirms good formation of the zeolitic material, exhibiting 2 to 5 μm crystals. In sample SZA (Fig. 7 (b)), in addition to the cube-shaped crystals typical of zeolite A, residual spherical particles from the ash used are also evident, confirming the presence of quartz in the sample obtained from fly ash. Despite the presence of these fly ash particles, zeolite A crystals are also visible in the micrograph, demonstrating good formation of the desired zeolitic material.

### 3.4. Textural properties

Textural analysis contributes to confirming the quality of zeolites formed and assesses properties such as specific surface area, pore volume and diameter. Table 4 presents the values of these properties for commercial zeolites (type X-CZX and type A-CZA), synthesized zeolites before and after the addition of binder to the conformation of the samples into spherical shapes, and the binder itself.

In the case of the zeolite NaA the change in the surface area from 36.87 to 39.40 is not a big change and could easily be attributed to variations in the analysis itself. However, to the NaX zeolite the role of the binder can be seen more clearly in the change of the surface area, since before the pelletization, the synthetic zeolite type NaX had a specific surface area similar to the commercial zeolite, 448.59 $m^2/g$ and 497.88 $m^2/g$, respectively. But after the pelletization with bentonite (52,63 $m^2/g$), the specific surface area dropped to 247.30 $m^2/g$, which corresponds around to 45% of the initial property.

Regarding to the pore volume properties the pelletization was not so compromising. Zeolite type NaX drops from 0.258 $cm^3/g$ to 0.205 $cm^3/g$ (about 20%) and type NaA remained constant.

Higher pore volumes can be observed for the commercial zeolites when compared to their synthetic counterparts, indicating better $CO_2$ adsorption capacity for the former. However, the values obtained for the synthetic zeolites also support their application in $CO_2$ adsorption and are consistent with those reported in the literature, where authors obtained surface areas of 249.7 $m^2/g$ and 397 $m^2/g$ for zeolite X and 15.7 and 10.9 $m^2/g$ for zeolite A [26], both synthesized from coal fly ashes. Nunes et al. [18] presented type NaX zeolite with 670 $m^2/g$ (commercial) and 423 $m^2/g$ (synthesized from coal fly ash). Ren et al. [19] synthesized type NaA zeolite from coal fly ash with 43.7 $m^2/g$ and Babajide [40] synthesized type NaX with 320 $m^2/g$.

It is important to underscore that textural properties are not the only factors that affect the $CO_2$ capturing capacity of adsorbent materials. At low pressures, the nature and density of cations also play an important role in $CO_2$ adsorption, since they provide active sites for capture, with sodium as a favorable cation for adsorption [18,41,42].

### 3.5. $CO_2$ adsorption

#### 3.5.1. Zeolite adsorption capacity

Fig. 8 presents the adsorption curves obtained from the TGA analysis for the four pelletized samples at 303 K. High $CO_2$ adsorption capacities were obtained for the synthesized zeolites, especially zeolite SZX (1.97 mmol/g), which displayed greater capture capacity in relation to SZA (1.37 mmol/g) and a capacity similar to that of the commercial zeolites. This indicates that the structure of zeolite SZX is well-defined as can be seeing through its XRD. Also, despite the reduction of some textural properties, the adsorption capacity before and after

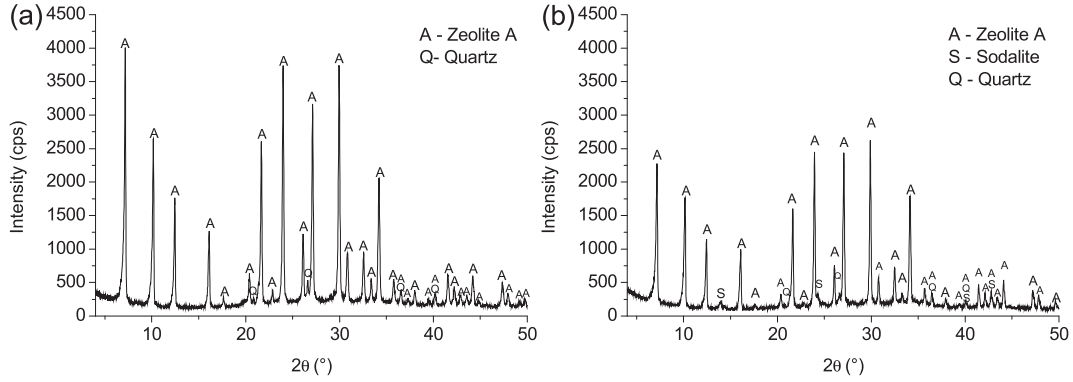


**Fig. 5.** X-ray diffractograms of the 4A (a) CZA and (b) SZA zeolites.

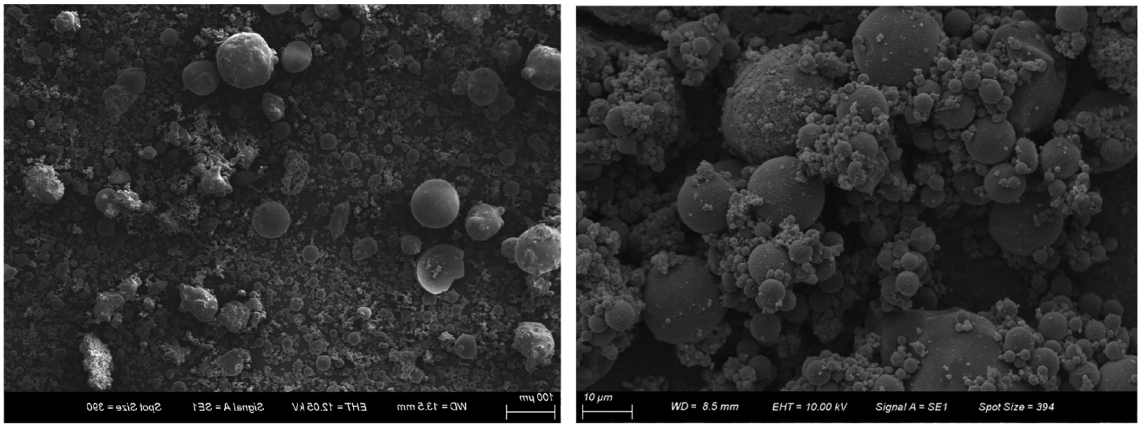


**Fig. 6.** Micrographs of the Jorge Lacerda (a) and Pecém (b) fly ash.

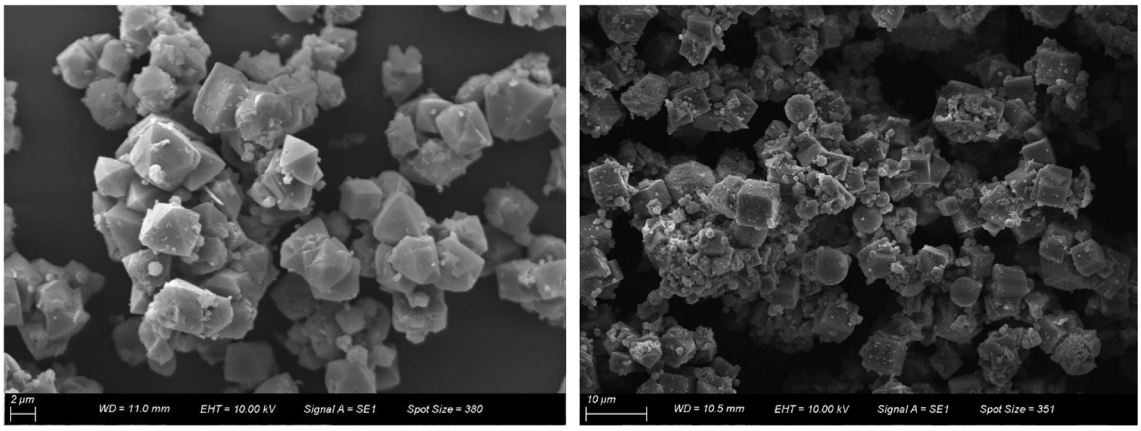


**Fig. 7.** Micrographs (SEM) of the synthetic SZX (a) and SZA (b) zeolites.

**Table 4**
Textural property results.

| Zeolite | Surface Area ($m^2$/g) | Pore Volume ($cm^3$/g) | Average Pore Diameter (Å) |
|---|---|---|---|
| CZX (pellet) | 497.80 | 0.349 | 28.060 |
| SZX (powder) | 448.59 | 0.258 | 23.050 |
| SZX (pellet) | 247.23 | 0.205 | 16.596 |
| CZA (pellet) | 27.56 | 0.138 | 100.498 |
| SZA (powder) | 36.87 | 0.099 | 43.783 |
| SZA (pellet) | 39.40 | 0.099 | 50.463 |
| Bentonite (binder) | 52.63 | 0.063 | 48.030 |

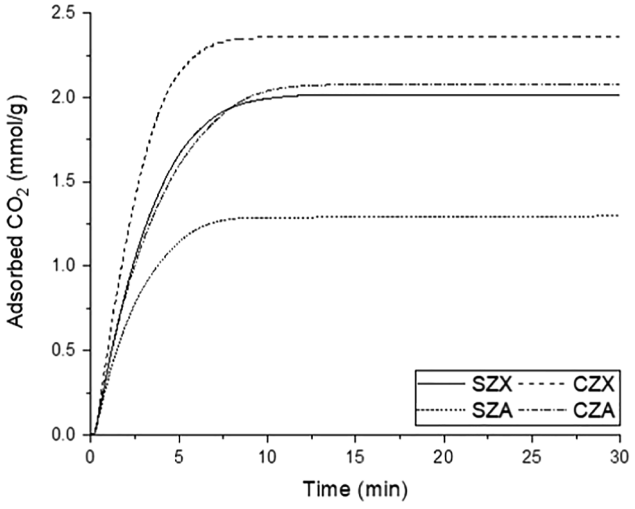


**Fig. 8.** Adsorption curves obtained for the four pelletized samples at 303 K.

pelletization, 2.15 mmol/g and 1.97 mmol/g to zeolite type NaX and 1.57 mmol/g and 1.37 mmol/g to type NaA, showed that this property was not greatly compromised in both cases.

Other studies with zeolites synthesized from coal fly ashes to access their adsorption capacity were already made. Kuceba and Nowak [5] used a TGA to measure de adsorption capacity in atmosphere of 10% $CO_2$ and reported similar results, presenting 1.18 mmol/g to zeolite type NaX synthesized from coal fly ash and 1.98 mmol/g for the commercial zeolite. Dantas [43] compared the same zeolite in atmosphere of 100% $CO_2$ and 20% $CO_2/N_2$ v/v and found capacities of 3.59 mmol/g and 2.49 mmol/g, respectively.

In addition to its smaller surface area and pore volume, the low $CO_2$ capture capacity of synthetic zeolite SZA may be related to the high concentration of cations with a charge greater than +1, such as Fe, Mg, Ca and Ti, whose combined content of 16.43% wt of the total sample (see Table 3) reduces $CO_2$ affinity [44]. A low Na concentration was also observed in the structure of the material, but its capacity is still deemed satisfactory when compared to other values reported in the literature [5,45].

Activation temperature is an important parameter to guarantee zeolite performance, since it allows greater dehydration and therefore higher $CO_2$ adsorption capacity. In their studies Kuceba and Nowak [5] applied different activation temperatures to the $CO_2$ adsorption using

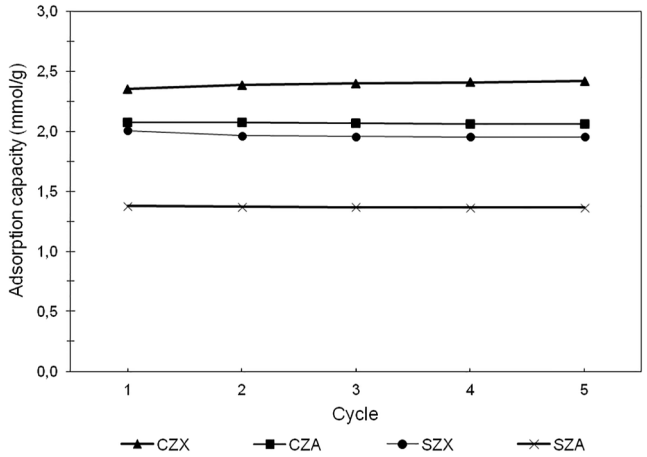


**Fig. 9.** Adsorption capacity of the commercial and synthetic zeolites in five adsorption/desorption cycles.

zeolites synthesized from coal fly ash and concluded that this parameter directly influences adsorption capacity. In this paper, the regeneration capacity of both the commercial and synthesized zeolites is also noteworthy, remaining almost constant after five adsorption/desorption cycles (Fig. 9), confirming their applicability in cyclic processes.

Even though this work hasn't a focus in the influence of moisture in the $CO_2$ adsorption, its well-known that flue gases also contain water vapor, which can greatly affect the adsorption capacity of $CO_2$ [5]. It happens because besides the competitive behavior between $CO_2$ and $H_2O$, the moisture can also block pores that were available to adsorption by surface adhesion (wetting action) and so occupying a certain amount of the adsorptive space [46].

### 3.5.2. Effect of temperature on adsorption capacity

Temperature is a determining factor in zeolite adsorption capacity, since gas adsorption is generally an exothermal phenomenon [3,5]. Fig. 10 demonstrates that adsorption capacity declined with a temperature increase from 303 K to 373 K in all the samples studied. The same behavior has also been reported in other studies [5,44].

In NaX and NaA zeolites, a rise in temperature from 298 K to 333 K resulted in a 20–30% decrease in adsorption capacity [41]. In the present study, a temperature increases from 303 K to 323 K prompted a 32.3% decline in $CO_2$ adsorption capacity for CZX, and 28.3, 26.6% and 14.1% for CZA, SZX and SZA, respectively. The results indicate a considerable reduction in adsorption capacity when the temperature

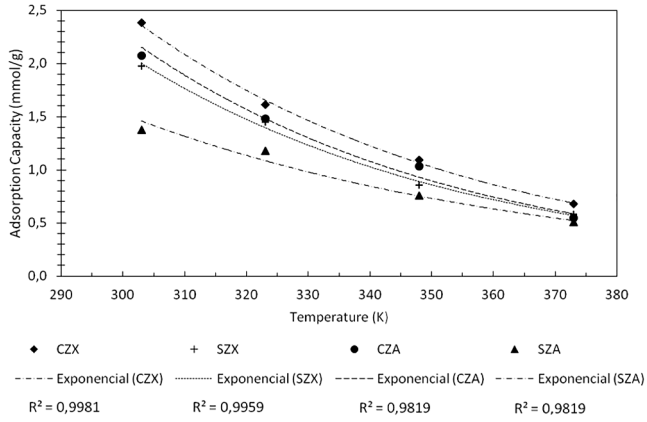


**Fig. 10.** Adsorption capacity of the commercial and synthetic zeolites at different adsorption temperatures.

increases, confirming the need for milder temperatures. In general, the commercial and synthetic zeolites showed similar behavior in terms of reduced adsorption capacity, with differences declining as the adsorption temperature increased.

Taking into account the application of these adsorbents in the already referred TSA cyclic process, changes in the adsorption temperature inside the adsorption section can easily occur.

### 3.5.3. Pure $CO_2$ adsorption isotherms

The equilibrium isotherms for the four samples are shown in Fig. 11. From these results It may be observed that the type X zeolites (Fig. 11a,b) show higher adsorption capacity than the type A zeolites (Fig. 11c,d) if compared at the same pressure (*e.g.* about 40% higher at 1 atm). Also, it should be noted that the synthesized samples, for both type X and type A zeolites, show in general very similar adsorption capacity values when compared to the values obtained for the commercial samples (within *ca.* 10% difference). These results follow the same behavior as those observed using the TGA analysis for $CO_2$ diluted in $N_2$, as reported in Section 3.5.1.

## 4. Conclusions

1. Although the binder used in the pelletization decreased the textural properties of the synthetic zeolite, good quality NaX and NaA samples were obtained from both coal fly ashes, exhibiting similar properties to the commercial zeolites, even the ash submitted to flue-gas desulfurization (Pecém). Their surface areas (247.23 $m^2/g$ for SZX and 39.4 $m^2/g$ for SZA), pore volumes (0.205 $cm^3/g$ for SZX and 0.099 $cm^3/g$ for SZA) are in accordance with those obtained from other synthetic zeolites.
2. The zeolites synthesized from coal fly ash displayed high $CO_2$ adsorption capacities (1.97 mmol/g for SZX and 1.37 mmol/g for SZA), with synthetic zeolite X exhibiting an adsorption capacity very similar to that of the commercial zeolites (2.39 CZX and 2.07 mmol/g CZA).
3. All the samples studied showed a high regeneration capacity after thermal activation, with their $CO_2$ capture capacity remaining almost unchanged after five adsorption/desorption cycles (loss < 3% for all samples), confirming their potential for application in TSA processes.
4. As observed in previous studies, adsorption analyses at different temperatures confirmed that $CO_2$ adsorption capacity is strongly influenced by and inversely proportional to temperature, justified by the exothermal nature of the process.
5. Pure $CO_2$ adsorption isotherms indicated that higher adsorption capacities for $CO_2$ were observed for the type X zeolites when compared to the type A zeolites. Also the synthesized zeolites from fly ash reported in this study presented $CO_2$ adsorption behavior similar to benchmark commercial 13X and 4A zeolite adsorbents.

## CRediT authorship contribution statement

**Thiago F. de Aquino:** Conceptualization, Methodology, Data curation, Writing - original draft, Writing - review & editing, Visualization, Supervision, Project administration, Funding acquisition. **Sabrina T. Estevam:** Conceptualization, Methodology, Investigation, Writing - original draft, Writing - review & editing. **Vanessa O. Viola:** Conceptualization, Investigation, Writing - original draft, Writing - review & editing. **Carolina R.M. Marques:** Writing - review & editing, Supervision, Project administration, Funding acquisition. **Fernando L. Zancan:** Visualization, Funding acquisition. **Lídia B. Vasconcelos:** Project administration, Funding acquisition. **Humberto G. Riella:** Writing - review & editing, Visualization. **Marçal J.R. Pires:** Writing - review & editing, Visualization. **Rafael Morales-Ospino:** Methodology, Investigation, Writing - review & editing. **A. Eurico B. Torres:** Methodology, Investigation, Writing - review & editing. **Moises Bastos-**

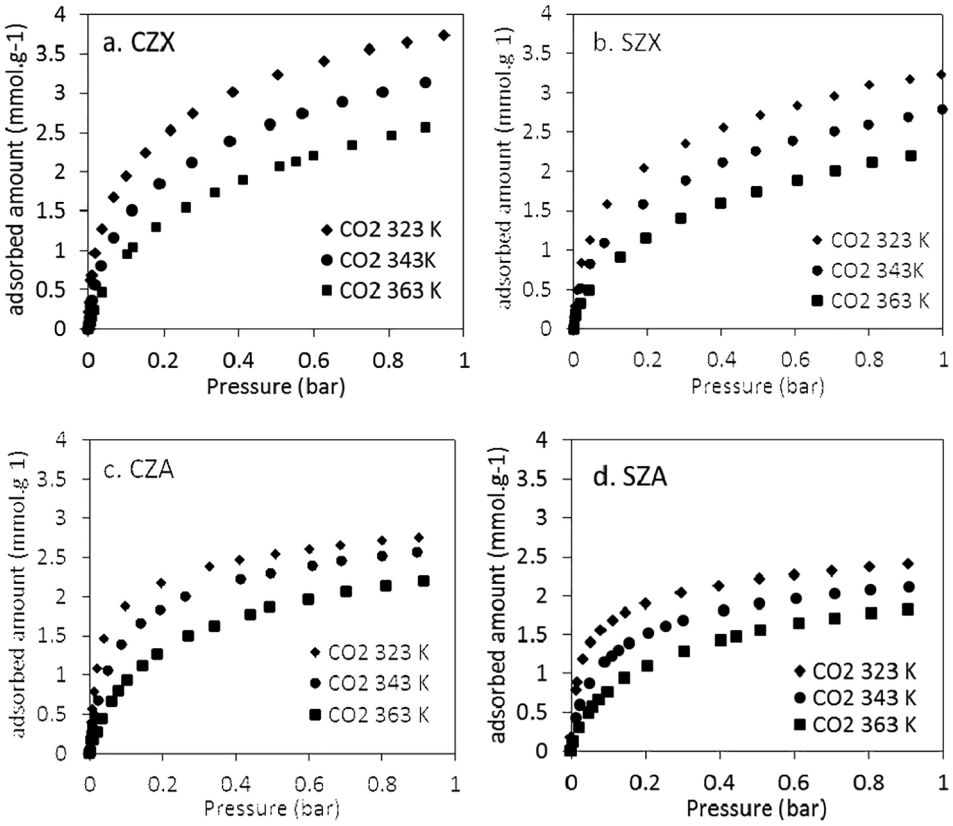


**Fig. 11.** Pure $CO_2$ adsorption isotherms at 323, 343 and 363 K up to 1 bar for CZX (a), SZX (b), CZA (c) and SZA (d) zeolites.

**Neto:** Methodology, Investigation, Writing - review & editing. **Célio L. Cavalcante:** Methodology, Investigation, Writing - review & editing.

## Declaration of Competing Interest

The authors declare that they have no known competing financial interests or personal relationships that could have appeared to influence the work reported in this paper.

## Acknowledgments

The authors are grateful to the ENEVA S.A. Corporation and FAPESC (Research Support Foundation of Santa Catarina State) for the funding provided.

## References

[1] Lima AEO. CO2 capture study using modified adsorbents via molecular simulation. Thesis, Master of Chemical Engineering, UFC. Brazil (Fortaleza); 2012. p.120. Portuguese.
[2] Kaithwas A, Prasad M, Kulshreshtha A, Verma S. Industrial wastes derived solid adsorbents for $CO_2$ capture: a mini review. Chem Eng Res Des 2012;90:1632–41.
[3] Wilcox J. Carbon capture. 1st ed. New York: Springer; 2012.
[4] Kim H, Miller DC, Moderjurti S, Omell B, Bhattacharyya D, Zitney SE. Mathematical modeling of a moving bed reactor for pos-combustion $CO_2$ capture. Process Syst Eng 2016;62:3899–914.
[5] Kuceba IM, Nowak W. A thermogravimetric study of the adsorption of $CO_2$ on zeolites synthesized from fly ash. Thermochim Acta 2005;437:67–74.
[6] Hefti M, Marx D, Joss L, Mazzotti M. Adsorption equilibrium of binary mixtures of carbon dioxide and nitrogen on zeolites ZSM-5 and 13X. Microporous Mesoporous Mater 2015;215:215–28.
[7] Aquino TF. Synthesis of type X zeolites from mineral coal fly and bottom ashes for $CO_2$ capture (Thesis) Brazil (Santa Catarina): Doctorate in Chemical Engineering UFSC; 2018. p. 170. Portuguese.
[8] Song H, Lei X, Xue F, Wu H, Cheng F. Composite phase-change coating with coal-fly-ash-based zeolite as carrier. Prog Org Coat 2019;136:105236.
[9] Yang T, Han C, Liu H, Yang L, Liu D, Tang J, et al. Synthesis of Na-X zeolite from low aluminum coal fly ash: characterization and high efficient As(V) removal. Adv Powder Technol 2019;30:199–206.
[10] Vadapalli VRK, Gitari WM, Ellendt A, Petrik LF, Balfour G. Synthesis of zeolite-P from coal fly ash derivative and its utilization in mine-water remediation. S Afr J Sci 2010;106:1–7.
[11] Liu Y, Yan C, Zhao J, Zuhua Z, Wang H, Zhou S, et al. Synthesis of zeolite P1 from fly ash under solvent-free conditions for ammonium removal from water. J Cleaner Prod 2018;202:11–22.
[12] Durairaj S, Vaithilingam S. Hydrothermal assisted synthesis of zeolite based nickel deposited poly(pyrrole-co-fluoro aniline)/CuS catalyst for methanol and sulphur fuel cell applications. J Electroanal Chem 2017;787:55–65.
[13] Park J, Hwang Y, Bae S. Nitrate reduction on surface of Pd/Sn catalysts supported by coal fly ash-derived zeolites. J Hazard Mater 2019;374:309–18.
[14] Cardoso AM, Horn MB, Ferret L, Azevedo CMN, Pires M. Integrated synthesis of zeolite 4A and Na-P1 using coal fly ash for application in the formulation of detergents and swine wastewater treatment. J Hazard Mater 2015;287:69–77.
[15] Hui KS, Chao CYH. Pure, single phase, high crystalline, chamfered-edge zeolite 4A synthesized from coal fly ash for use as a builder in detergents. J Hazard Mater 2006;137:401–9.
[16] Li J, Zhuang X, Font O, Moreno N, Vallejo VR, Querol X, et al. Synthesis of merlinoite from Chinese coal fly ashes and its potential utilization as slow release K-fertilizer. J Hazard Mater 2014;265:242–52.
[17] Flores CG, Shneider H, Marcilio NR, Fernet L, Oliveira JCP. Potassic zeolites from Brazilian coal ash for use as a fertilizer in agriculture. Waste Manage 2017;70:263–71.
[18] Nunes APB, Sennour R, Arus VA, Anoma S, Pires M, et al. $CO_2$ capture by coal ash-derived zeolites- roles of the intrinsic basicity and hydrophilic character. J Alloy Compd 2019;778:866–77.
[19] Ren X, Xiao L, Qu R, Liu S, Ye D, Song H, et al. Synthesis and characterization of a single phase zeolite A using coal fly ash. R Soc Chem 2018;8:42200–9.
[20] Hedin N, Andersson L, Berström L, Yan J. Adsorbents for the post-combustion capture of $CO_2$ using rapid temperature swing or vacuum swing adsorption. Appl Energy 2012;104:418–33.
[21] Yoldi M, Fuentes-Ordones EG, Korili SA, Gil A. Zeolite synthesis from industrial wastes. Microporous Mesoporous Mater 2019;287:183–91.
[22] Breck DW. Zeolite molecular sieves: structure, chemistry, and use. 1st ed. New York: Wiley; 1974.
[23] Melo CR, Riella HG, Kuhnen NC, Angioletto E, Melo AR, Bernardin AM, et al. Synthesis of A zeolites from kaolin for obtaining A zeolites through ionic exchange for adsorption of arsenic. Mater Sci Eng, B 2012;177:345–9.
[24] Bortolatto LB, Boca Santa RAA, Moreira JC, Machado DB, Martins MA, Fiori MA, et al. Synthesis and characterization of Y zeolites from alternative silicon and aluminium sources. Microporous Mesoporous Mater 2017;248:214–21.
[25] Mohamed RM, Mkhalid IA, Barakat MA. Rice husk ash as renewable source for the production of zeolite NaY and its characterization. Arabian J Chem 2015;8:48–53.

[26] Izidoro CI, Fungaro DA, Abbott JE, Wang S. Synthesis of zeolites X and A from fly ashes for cadmium and zinc removal from aqueous solution in single and binary ion systems. Fuel 2012;103:827–34.
[27] Cardoso AM, Paprocki A, Ferret LS, Azevedo CMN, Pires M. Synthesis of zeolite Na-P1 under mild conditions using Brazilian coal fly ash and its application in wastewater treatment. Fuel 2015;139:59–67.
[28] Izidoro JC. Synthesis and characterization of pure zeolite obtained from coal fly ash. Thesis Doctorate in Science in the area of Nuclear Technology – Materials, IPEN. Brazil (São Paulo), 2013. p. 146. Portuguese.
[29] Shigemoto N, Hayashi H, Miyaura K. Selective formation of Na-X zeolite from coal fly ash by fusion with sodium hydroxide prior to hydrothermal reaction. J Mater Sci 1993;28:4781–6.
[30] Querol X, Alastuey A, López-Soler A, Plana F. A fast method for recycling fly ash: microwave-assisted zeolite synthesis. Environ Sci Technol 1997;31:2527–33.
[31] Iqbal A, Sattar H, Haider R, Munir S. Synthesis and characterization of pure phase zeolite 4A from coal fly ash. J Cleaner Prod 2019;219:258–67.
[32] Izidoro JC, Fungaro DA, Santos FS, Wang S. Characteristics of Brazilian coal fly ashes and their synthesized zeolites. Fuel Process Technol 2012;97:38–44.
[33] Depoi FS, Pozebon D, Kalkreuth WD. Chemical characterization of feed coals and combustion-by-products from Brazilian power plants. Coal Geol 2008;76:227–36.
[34] Rohde GM, Machado CS. Quantification of fossil coal ashes produced in Brazil. Rio Grande do Sul (RS): Rio Grande do Sul Science and Technology Foundation, Secretariat of Science, Innovation and Technological Development; 2016 Jul. Report No.:36. Sponsored by Rio Grande do Sul Government. Portuguese.
[35] Sulayon AH, Mahdi AS. Spherical Zeolite-Binder agglomerates. IChem 1999;77:342–50.
[36] Saha S, Wiebcke M, Huber K. Insight into fast nucleation and growth of zeolitic imidazolate framework-71 by in situ static light scattering at variable temperature and kinetic modeling. Cryst Growth Des 2018;18:4653–61.
[37] Sun H, Shen B, Liu J. N-Paraffins adsorption with 5A zeolites: the effect of binder on adsorption equilibria. Sep Purif Technol 2008;64:135–9.
[38] Inada M, Eguchi Q, Enomoto N, Hojo J. Syntheses of zeolite from coal fly ashes with different silica-alumina composition. Fuel 2005;84:299–304.
[39] Mainganye D, Ojumu TV, Petrik L. Synthesis of zeolites Na-P1 from South Africa coal fly Ash: effect of impeller design and agitation. Materials 2013;6:2074–89.
[40] Babajide O, Musyoka N, Petrik L, Ameer F. Novel zeolite Na-X synthesized from fly ash as a heterogeneous catalyst in biodiesel production. Catal Today 2012;190:54–60.
[41] Haucchum L, Mahanta P. Performance enhancement of $CO_2$ capture from flue gas in a bubbling fluidized bed. J Energy Inst 2016;90:764–75.
[42] Martin-Calvo A, Parra JB, Ania CO, Calero S. Insights on the anomalous adsorption of carbon dioxide n LTA zeolites. J Phys Chem 2014;118:25460–7.
[43] Dantas TLP. Carbon dioxide separation by adsorption from synthetic mixtures of the exhaust gas type. Thesis, Doctorate in Chemical Engineering, UFSC. Brazil (Santa Catarina); 2009. p. 159. Portuguese.
[44] Bonenfant D, Kharoune M, Niquette P, Mimeault M, Hausler R. Advances in principal factors influencing carbon dioxide adsorption on zeolites. Sci Technol Adv Mater 2008;9:1–7.
[45] Yi H, Deng H, Tang X, Yu Q, Zhou X, Liu H. Adsorption equilibrium and kinetics for $SO_2$, NO, $CO_2$ on zeolites FAU and LTA. J Hazard Mater 2011;203–204:111–7.
[46] Zhang ZG, Cao SG, Li Y, Guo P, Yang H, Yang T. Effect of moisture content on methane adsorption and desorption-induced deformation of tectonically deformed coal. Adsorpt Sci Technol 2018;36:548–68.